Solar Energy Materials & Solar Cells 274 (2024) 112993

Contents lists available at ScienceDirect

Solar Energy Materials and Solar Cells

journal homepage: www.elsevier.com/locate/solmat

Low-temperature influence on the properties and efficiency of thin-film perovskite solar cells fabricated by the PVco-D technique

Anna Zawadzka [a,b,*], Agnieszka Marjanowska [a,b], Amina Laouid [a,b,c], Krzysztof Wisniewski [a], Youssef El Kouari [d], Youssef El Hani [d], Przemysław Płóciennik [b,e]

[a] Institute of Physics, Faculty of Physics, Astronomy, and Informatics, Nicolaus Copernicus University in Torun, Grudziadzka 5, PL 87-100, Torun, Poland
[b] Centre for Modern Interdisciplinary Technologies, Nicolaus Copernicus University in Torun, Wilenska 4, PL 87-100, Torun, Poland
[c] Chouaib Doukkali University of El Jadida, National School of Applied Sciences, Engineering Science for Energy Lab, El Jadida, Morocco
[d] Laboratory of Physics of Condensed Matter and Renewable Energy, Faculty of Sciences and Technology, Hassan II University of Casablanca, B.P 146, Mohammedia, Morocco
[e] Institute of Engineering and Technology, Faculty of Physics, Astronomy, and Informatics, Nicolaus Copernicus University in Torun, Wilenska 7, PL 87-100, Torun, Poland

ARTICLE INFO

Keywords:
Physical vapor co-deposition (PVco-D)
Methylammonium lead iodide thin films
Perovskite solar call
Phase transition
Low-temperature characterization

ABSTRACT

The study discussed in this publication aimed to develop a perovskite solar cell adapted to operating conditions at reduced temperature and pressure and less than 1 μm thick. The physical vapor co-deposition technique was proposed and successfully used to create a solar cell structure with a thin layer of hybrid perovskite as an energy-collecting material. A comprehensive analysis of methylammonium lead iodide behavior in a wide temperature range from 10 K to 320 K was carried out to implement this project. The initial phase included assessing the degradation of the perovskite material layer after cooling to the temperature of liquid helium and then re-heating it to room temperature. Then, using spectroscopic techniques, the characteristics of the layers' optical and electrical properties were determined. The obtained results allowed the design of the complete structure of a thin-film perovskite cell, which was made using only the vacuum sublimation process. Simulations using the SCAPS-1D program and experimental results showed high agreement and allowed for obtaining an efficiency of approximately 18.5 % in the interested temperature range. Perovskite solar cell stability tests over six months confirmed the positive impact of the proposed technique for depositing the complete cell structure on its temporal stability. The research results are optimistic for the applications of perovskite cells in space.

1. Introduction

The unique photo-electro-physical properties of hybrid organic-inorganic halide perovskites have contributed to diverse studies on these promising solar cell materials over the last dozen years [1–4]. Although these compounds were first described almost 40 years ago [5], research into the characterization of their properties and applications in optoelectronic and photovoltaic devices is much more recent [6–8]. Despite the tremendous effort many researchers have put into characterizing these materials, more fundamental knowledge still needs to be underlying their unique properties. This is especially true for organic-inorganic complexes, which are often compounds with mixtures of organic and metal cations and halide anions with refined surfaces and interfaces [9,10]. Their nature and occurrence are essential, especially if the perovskite is a thin film with a thickness equal to several hundred nanometers. These thin-film materials are most desirable in opto- and photovoltaic devices, contributing to their miniaturization. Among the family of hybrid halide perovskites, methylammonium lead iodide ($CH_3NH_3PbI_3$ or $MAPbI_3$) is still the most important due to its unique optoelectronic properties, including high carrier mobility, long carrier lifetime, low carrier recombination coefficient, long exciton diffusion length, and high absorption coefficient in the ultraviolet and visible range [11,12].

A perovskite thin film solar cell (PTFSC) includes a thin film of the perovskite-structured compound, most commonly a halide-based material as the light-harvesting active film. Perovskite materials, such as

* Corresponding author. Institute of Physics, Faculty of Physics, Astronomy, and Informatics, Nicolaus Copernicus University in Torun, Grudziadzka 5, PL 87-100, Torun, Poland.
E-mail address: azawa@fizyka.umk.pl (A. Zawadzka).

https://doi.org/10.1016/j.solmat.2024.112993
Received 31 January 2024; Received in revised form 7 June 2024; Accepted 10 June 2024
Available online 14 June 2024
0927-0248/© 2024 Elsevier B.V. All rights are reserved, including those for text and data mining, AI training, and similar technologies.

methylammonium lead halides and completely inorganic metal halides, have become extremely popular in the last decade as candidate materials for practical solar cell applications due to their low cost and simplicity in production. The efficiency of solar cells with single-junction architectures in laboratory devices using these materials has increased from 3.8 % in 2009 [13] to 25.7 % in 2021 [14], and in silicon-based tandem cells up to 30 % [15,16], exceeding the maximum efficiency achieved in single-junction silicon solar cells. Therefore, as of 2016, perovskite solar cells are the fastest growing solar cell technology [17].

The primary technique used to obtain $MAPbI_3$ layers is the spin-coating technique. In this technique, the layer is obtained after placing a drop of solution on the surface of the substrate and then rotating it at 10^3 rot/min while heating it to a temperature above 90 °C. All precursors of the appropriate perovskite are contained in the solution used [18,19]. The advantage of the spin-coating technique is undoubtedly its simplicity. This technique also has many drawbacks, such as the lack of repeatability of the physical parameters of the layers and the lack of control over the structural properties during the layer formation process, dramatically limiting the commercial application possibilities in optoelectronic and photovoltaic devices. The search for new techniques for producing thin films of hybrid perovskites is crucial for commercial applications. Therefore, in this work, we used our innovative technique - a physical high vacuum co-deposition (PVco-D) process based on the vapor phase deposition technique. The PVco-D technique allows for unprecedented layer uniformity on a large scale, complete repeatability, and process control [20–22]. Many identical samples were obtained in one process with consistent physical properties. The obtained results suggest that this innovative technique is up-and-coming for practical applications.

The challenges to the fundamental understanding of the optical and electrical properties of $MAPbX_3$ perovskites arise from their rich microstructural nature and their intertwinement. Therefore, in this article, we decided to undertake research on explaining and completing the optical and electrical properties of $CH_3NH_3PbI_3$ thin films deposited by using PVco-D technique, paying particular attention to the structural properties and interconnections of physical properties in a wide temperature range from 10 to 320 K.

This work presents not only experimental research but also theoretical studies that became possible thanks to obtaining the unique uniformity of the layers. First, it allowed us to obtain characteristics of optical parameters such as refractive index, absorption coefficient, extinction coefficient, and complex dielectric constant. Additionally, it allowed for a comprehensive examination of various crystallographic phases of the tested perovskite, characterized not only by a different structure of the unit cell but also by a significant change in the optical energy gap and its behavior, different from the typical semiconductors, as a function of the temperature. Finally, the results obtained from the research on the behavior of thin perovskite layers allowed the design and optimization of the structure of a solar cell using perovskite as an energy-harvesting material. A wide range of temperature tests allowed us to assess the possibilities and estimate the efficiency of cells working in low-temperature and low-pressure conditions.

2. Experiment

The $CH_3NH_3PbI_3$ thin films were fabricated by using the Thin Film Deposition System - NANO 36™ (Kurt J. Lesker Company) [23,24] and the Physical Vapor co-Deposition (PVco-D) technique. The co-deposition process is an original technical solution of the research team, and its use allowed the obtaining of thin films of different hybrid perovskites with unprecedented homogeneity over a large surface. The adaptation of commercially available equipment to the co-deposition process was carried out in cooperation Kurt J. Lesker Company.

The proposed co-deposition process involved the simultaneous use of two independent thermal sources. A metal halide (lead iodide) was placed in one source in the presented investigation. The second source contained methylammonium halide (methylammonium iodide). Each of the two sources was independently controlled during the whole layer deposition process. The possibility of placing two different materials in two independent thermal sources is of great importance in obtaining hybrid organic-inorganic materials in the form of thin films. As is commonly known, organic and inorganic materials have completely different parameters when subjected to thermal processes. Organic materials are usually characterized by a much lower temperature of the melting and vapor points [25,26].

Very often, too high a temperature in the physical vapor deposition process leads to the decomposition of the organic compound rather than its vacuum sublimation. In the case of methylamine iodide, the temperature of the thermal source should not exceed 90 °C in the high vacuum condition to prevent the breakdown of chemical bonds. The vacuum sublimation process is stable for inorganic materials such as metal halides, and the compound does not decompose. However, this material requires a much higher temperature in the sublimation process in high vacuum conditions, namely 240 °C. Therefore, the PVco-D process is the only solution to obtain thin films of hybrid perovskites. In the normal PVD process, the compound decomposes. Initially, the lower temperature component is deposited, and then the higher temperature component. The final result will not be a hybrid layer but a system of two layers - organic and inorganic. In order to carry out the PVco-D deposition process, it is necessary to use a high vacuum for two reasons: to ensure conditions for the sublimation of components and thermal insulation of independent sources. The deposition process was carried out inside a vacuum chamber under pressure of about $1*10^{-6}$ Tr.

The source material was thermally evaporated from tungsten thermal sources and aluminum oxide or quartz crucible cells with a nozzle of 10 mm diameter on the top. The distance between the source and substrate was equal to 20 cm, and the substrates were held at room temperature and rotated with a speed equal to 20 rpm, thanks to which uniform layers were obtained on a large scale. Two independent piezoelectric controllers controlled both sublimated materials' deposition rate and thickness during the whole deposition process. The shutters opened only after reaching the appropriate rate for both materials to allow deposition on the substrates. Investigated hybrid perovskite thin films were deposited on BK7 glass substrates. Ultimately, homogeneous films with a dark brown color typical for the tested perovskite were obtained. Taking into account the colors of thin layers of components in thermal sources, namely methylammonium iodide - colorless and lead iodide - yellow, it can be concluded that the conditions inside the vacuum chamber proposed in the experiment allowed the formation of perovskite layers on the substrate surface. The films discussed in this work were 540 nm thick. Fig. 1 shows the idea of the PVco-D process and reflects the structure of the vacuum chamber in the experiment.

3. Material

First three-dimensional (3D) organic–inorganic hybrid perovskite, discovered by replacing cesium in $CsPbX_3$ (X = Cl, Br or I) with methylammonium cations ($MA = CH_3NH_3^+$) by Dieter Weber, in 1978 [27]. Its photovoltaics application was discovered almost thirty years later. In 2009, Kojima and co-workers described organometallic perovskite solar cells in which methylammonium lead halide (X = I, Br) solutions were deposited on the surface of a mesoporous titanium dioxide layer by spin casting technique [28]. Although the efficiency achieved by their cells was at most 5 %, they initiated great interest in research on various perovskites and their applications in optoelectronics and photovoltaics. Today, many researchers worldwide are trying to develop new perovskites to increase the efficiency of solar cells. The number of scientific publications exceeds several thousand per year.

Hybrid organic-inorganic halide perovskites are described by the same general formula AMX_3 as other compounds belonging to the perovskite family. In this formula for methylammonium lead iodide, A is

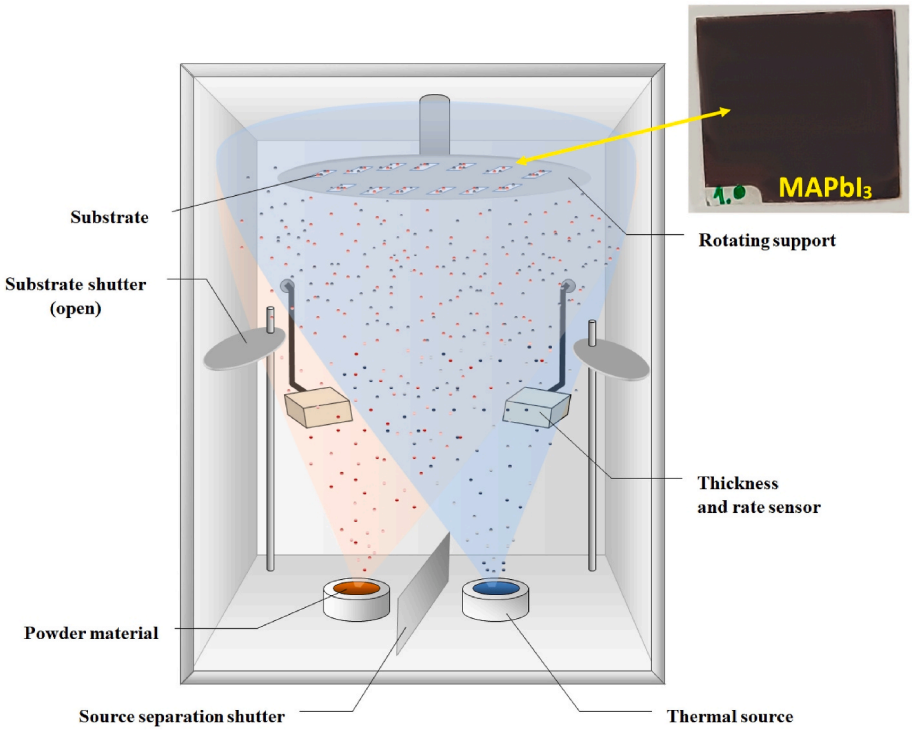


Fig. 1. Vacuum chamber of the PVco-D apparatus.

a non-bonding monovalent organic cation (methylammonium cation – $CH_3NH_3^+$), M is an octahedral coordinated divalent metal ion (lead cation – Pb^{2+}), and X is a monoanion halide ion selected primarily from elements such as bromine, chlorine, or iodine (iodide anion, I^-), as presented in Fig. 2a.

All hybrid organic-inorganic halide perovskites can exist in three crystallographic phases: cubic, tetragonal, and orthorhombic, depending on the temperature of the surrounding environment. However, each perovskite is characterized by different phase transition temperatures. Methylammonium lead iodide has a tetragonal crystal structure at room

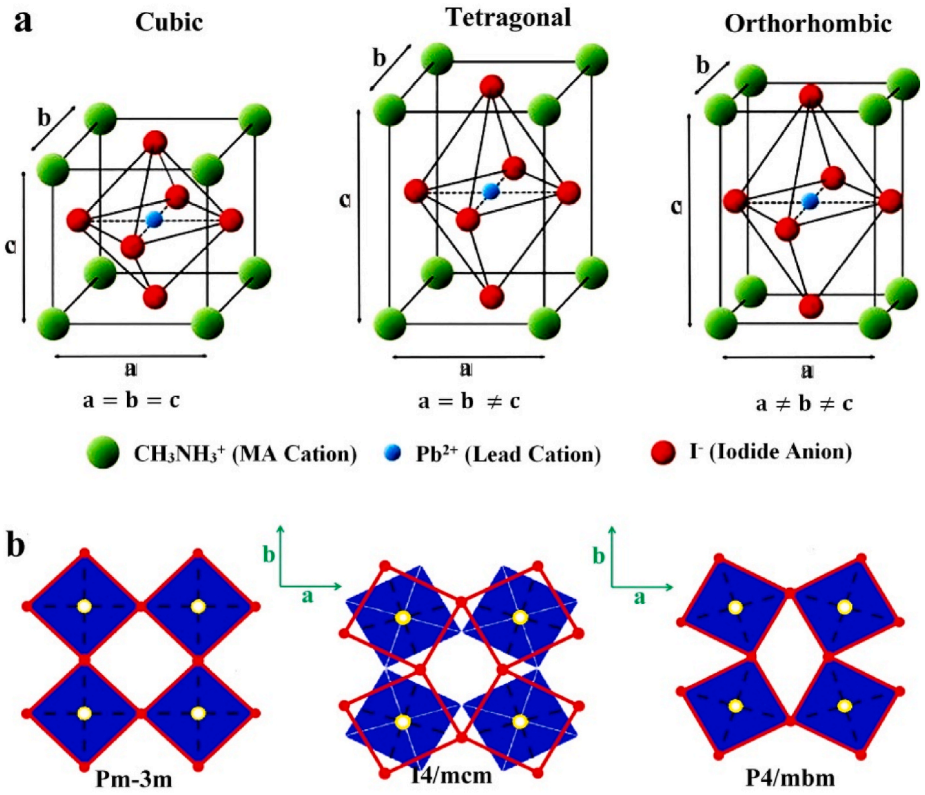


Fig. 2. The crystal structures of $MAPbI_3$: presentation of crystallographic phases and unit cell (a) and space group (b).

temperature, which distinguishes it from other halides (bromide or chloride), which are in the cubic phase at room temperature. The transition to the cubic phase occurs at a temperature slightly higher than room temperature, around 330–350 K. The transition to the orthorhombic phase will occur at a temperature lower than room temperature, approximately 140–160 K [29,30]. Table 1 contains parameters describing the unit cell for all crystallographic structures in which perovskite can occur.

The structural phase transitions in $MAPbI_3$ are similar to other inorganic perovskites such as $CsPbI_3$. Therefore, essential features of the phase transitions in $MAPbI_3$ may still be described using the formalism developed for inorganic perovskites.

The main component of these phase transitions is the rigid rotation of the PbI_6 octahedron. Octahedrons have joint angles, so rotation in a direction perpendicular to the axis of rotation must be out of phase. However, they can be in or out of phase in a direction parallel to this axis. If the rotation of the octahedron along that axis is in phase, the parameters describing the unit cell along that axis do not change. When rotation is out of phase, the unit cell parameters change. These pure tilt transitions are located at the boundaries of the Brillouin zone (BZ) of the cubic unit cell: in phase rotation at point M = (½ ½ 0) and out of phase rotation at point R = (½ ½ ½). When the octahedron undergoes rotations that are not entirely in or out of phase, the transition occurs along the line T connecting the M and R points of the BZ. As these phase transitions create new lattice vectors and larger unit cells, the M or R point folds to the Γ point in the lower symmetry phase (the M or R point has *P4/mbm* or *I4/mcm* symmetry) [31,32]. Therefore, as the temperature decreases, the symmetry of the crystallographic structure decreases.

Fig. 2b shows the positions of the octahedrons at subsequent phase transitions. Relative rotation of adjacent layers of PbI_6 octahedron along the c-axis is shown as filled blue squares and unfilled red squares. In the cubic Pm-3m structure, the octahedron does not rotate. In the I4/mcm structure, adjacent planar octahedrons rotate in opposite directions along the c-axis. Meanwhile, in the P4/mbm structure, adjacent octahedral planes rotate in the same direction along the c-axis.

4. Physical properties of the $MAPbI_3$ thin films

4.1. Atomic force microscopy - investigation of the microstructure and surface of the layer

Atomic force microscopy measurements were performed to determine the films' surface roughness and structural properties. AFM imaging was performed in contact mode using a NanoSurf EasyScan 2 instrument equipped with a Sicon-a cantilever [33,34]. Fig. 3a and b shows typical AFM images of the $CH_3NH_3PbI_3$ thin film surface obtained using the PVco-D process. The images show the surface of the layer immediately after deposition on the glass substrate and after measuring temperature changes in physical properties related to the phase transitions of the tested material.

Table 1
$MAPbI_3$ unit cell parameters for different crystallographic structures [30–32].

Phase	a (Å)	b (Å)	c (Å)	Description
Orthorhombic	9.04	12.66	8.35	DFT/PBEsol PND (100 K)
	8.87	12.63	8.58	Experiment
	8.84	12.58	8.56	
Tetragonal	8.70	8.72	12.83	DFT/PBEsol PND (100 K)
	8.81	8.81	12.71	Experiment
	8.8; 8.85	8.8; 8.85	12.68; 12.44	
Cubic	6.29	6.23	6.37	DFT/PBEsol PND (100 K)
	6.32	6.32	6.32	Experiment
	6.258; 6.312	6.258; 6.312	6.34; 6.316	

AFM images show that the structure of the layer is microcrystalline, and the size of the crystallites ranges from 200 to 300 nm. Although there is a slight reduction in roughness and crystallite size, no significant change in the structure of the layer was observed after cooling to 10 K and reheating to room temperature.

Detailed analysis used the Minkowski function method (MFM) [reference] to characterize the experimental data on the textured surfaces [35,36]. It will enable us to analyze the spatial distribution of the sites of holes (or valleys) in detail. MFs are one of the best alternatives to structure functions. Further, they are connected to physically functional parameters like the percolation threshold.

Normalization by total analysis area is necessary to quickly compare the functions determined for images of different scan ranges. At each level h of the topography level set, N_B and N_W represent black and white pixels, $N_{Bounded}$ are boundary pixels, and n_B and n_W, are isolated regions or islets. Black pixels represent material points (bulk or surface) and white pixels represent void points (air). The first function measures the relative amount of material present below level h. The plot is the bearing area curve or Abbott-Firestone curve and is used to calculate the functional roughness parameters.

The first MF (Minkowski volume) V is the coated surface area at level h and is defined as:

$$V(h) = \frac{N_B}{N_B + N_W}, \tag{1}$$

and the second MF (Minkowski Boundary) B is the length of contours:

$$B(h) = \frac{N_{Bounded}}{N_B + N_W}. \tag{2}$$

This function describes the shape of the microstructure surface feature. The second function for a level set with multiple or spiky isolated regions is larger than for a set with few or smooth regions. Finally, the third MF (Minkowski connectivity) χ, also called the Euler characteristic, is defined as:

$$\chi(h) = \frac{n_B - n_w}{N_B + N_W}. \tag{3}$$

The Euler characteristic represents the connectivity of the spatial pattern. A negative Euler characteristic indicates that the surface is characterized primarily by isolated holes (i.e., porous structures). Instead, a positive Euler characteristics indicate that the surface is primarily composed of isolated hills (i.e., island structures). Further, the maximum value of χ is equal to the maximum density of peaks and the minimum χ, the maximum density of valleys. Fig. 4a–d presents the height distribution and Minkowski Functionals of the $CH_3NH_3PbI_3$ thin films.

The percolation threshold determined using MFs was approximately 0.6 and did not change significantly (3 % increase) after cooling and reheating the sample. This means that up to 60 % of the layer thickness on the substrate side has a compact microstructure. However, above it has a much more porous microstructure. The obtained AFM images as well as their detailed characterization based on Minkowski functionals before and after the cooling process allow us to assume that thin films should retain their physical properties after returning to the primary (tetragonal) phase.

4.2. Transmission and reflection in thin films and its temperature dependence

Knowledge of the optical constants of thin films is crucial, especially from the point of view of their application possibilities, e.g., in optical or optoelectronic devices. These values can be determined using various combinations of transmission and reflection measurements [37]. The simplest way to determine these optical constants is to perform at least

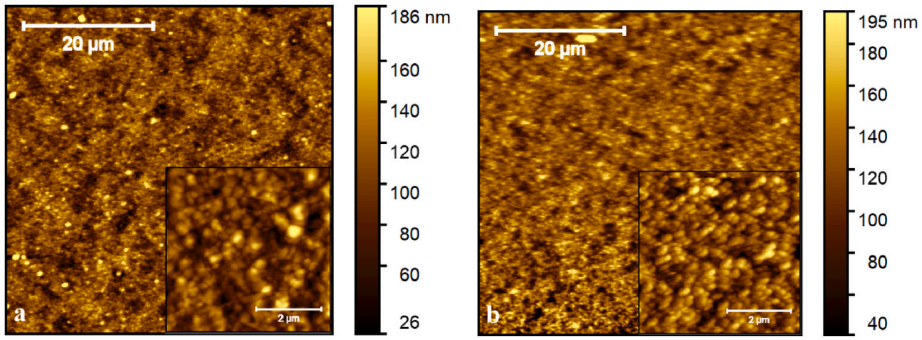


Fig. 3. AFM image of $MAPbI_3$ thin film: as deposited sample (a) and after cooling to the 10 K (b).

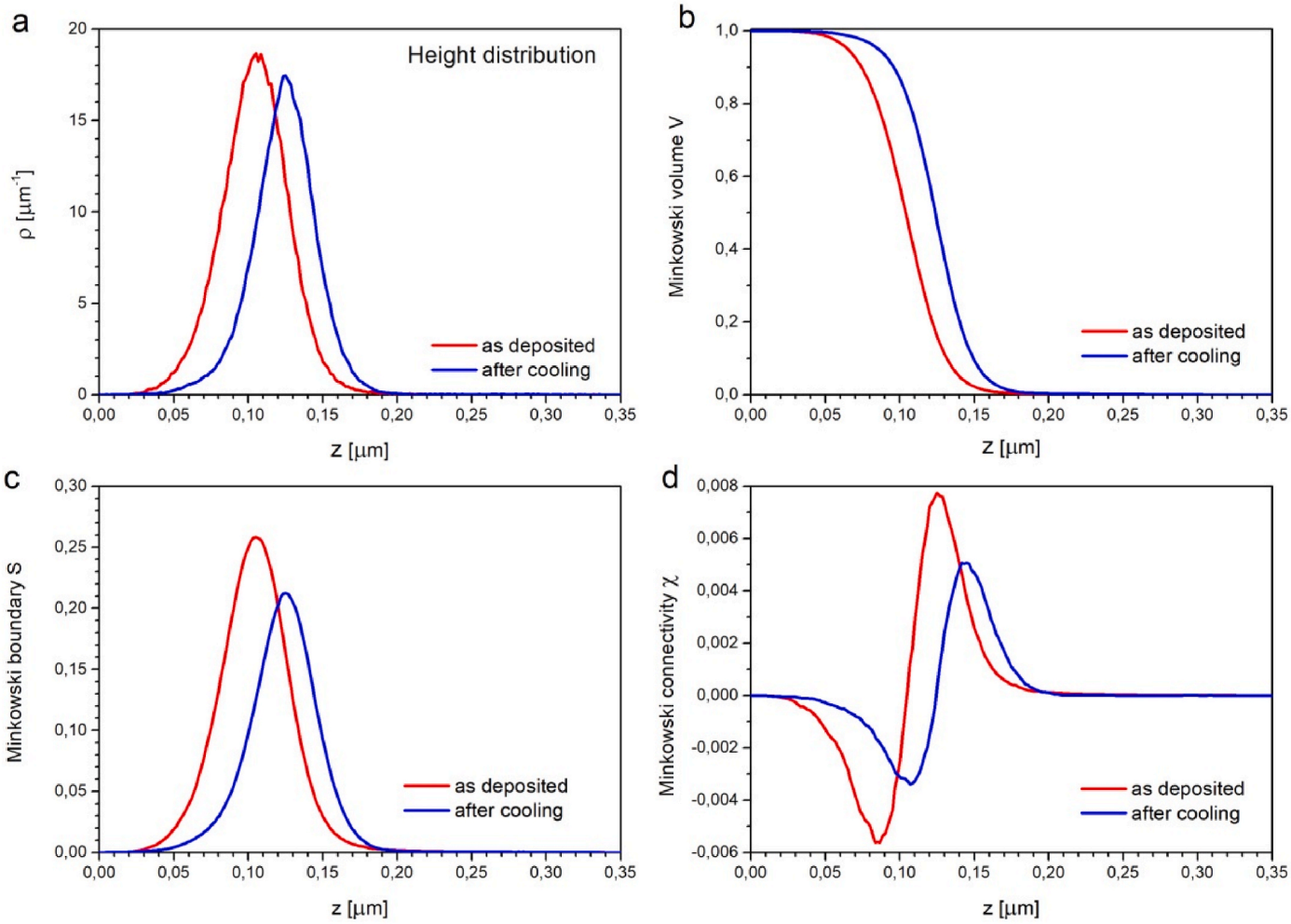


Fig. 4. Height distribution (a) and MFs of the halide perovskites thin film: Minkowski Volume (b), Minkowski Boundary (b) and Minkowski Connectivity (d).

two independent measurements of the transmission and reflection coefficients [38,39]. A more complicated method is the transmission or reflection spectrum envelope method. Regardless of whether transmission or reflection spectra will be used to determine a thin layer's optical constants, it is necessary to know the analytical relations linking the experimentally determined parameters and optical constants of the tested material.

To determine these relationships, let's consider a thin layer of material that absorbs radiation deposited on a much thicker substrate, as shown in Fig. 5. This structure is located in the air, and each of the materials (i.e., layer and substrate) is described by the complex refractive index $\tilde{n} = n - i\kappa$, where n is its real part, and κ is the extinction coefficient ($\alpha = 4\pi\kappa/\lambda$) - its imaginary part. The real part of the substrate's refractive index is smaller than the refractive index of the film, the film's thickness is d, the thicknesses of both media are the same everywhere and the radiation falls on the system from the side of the film.

Two reflected beams will be created above the film's surface: one resulting from reflection from the upper surface of the film and the other from its lower surface. Passing through the air-layer boundary and exiting the layer, the second beam is refracted. Analogous radiation behavior will occur at every boundary of the media. Thus, in addition to these two beams above the film, there are beams from triple, quintuple and further reflections from both layer surfaces. These beams can

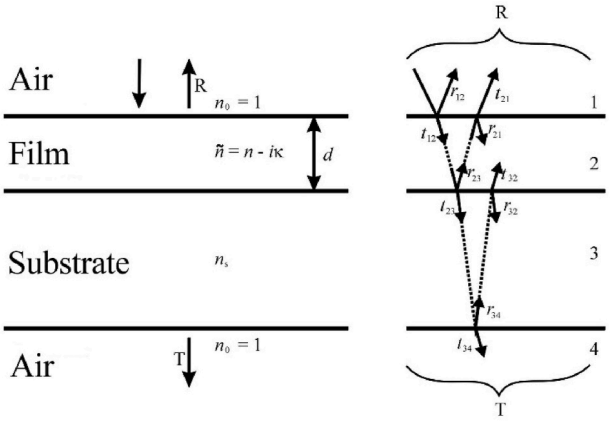


Fig. 5. A diagram showing the reflection and transmission of radiation falling on a system consisting of an absorbing thin layer and a non-absorbing substrate surrounded by air: d – thickness of the film, n, κ – its refractive and extinction coefficients, n_s – refractive index of the substrate, r_{ij} – amplitude reflection coefficients, t_{ij} – amplitude transmission coefficients.

interfere with each other, and this interference is both constructive and destructive. As a result, the reflection spectrum is characterized by strong oscillations, which may additionally be superimposed by beams reflected from both surface boundaries. Similar oscillations will be observed for the interference of beams passing through the tested system.

Suppose reflection occurs from a surface separating an optically rarer medium (with a lower refractive index) from an optically denser one (with a higher refractive index). In that case, the electromagnetic radiation beam undergoes a phase shift π during reflection. The beam is reflected without phase change if the density dependence is reversed. In both cases, the phase of the transmitted beam does not change. Taking into account the difference in the length of optical paths for rays reflected from the upper and lower surfaces of the film and the phase changes during reflection, it is possible to describe the conditions under which interference will be constructive or destructive:

$$2dn = \left(m + \frac{1}{2}\right)\lambda, \text{constructive interference} \tag{4a}$$

$$2dn = m\lambda, \text{destructive interference} \tag{4b}$$

In the case of the transmission spectrum, the situation will be the opposite, i.e., where there is a minimum for reflection, a maximum for transmission appears. Both of the above equations express the order of interference. The factor in equation (4a) results from the phase change during reflection from a denser medium. The phase change of π is equivalent to a difference in optical paths equal to half the wavelength of the incident radiation.

To determine the optical constants for a system of the homogeneous film with a thickness d deposited on a transparent substrate, surrounded by air (Fig. 5) and transmitted radiation, the transmission and reflection coefficients described by the following relations can be used:

$$R = \frac{A' - \left[B'_1\cos(2\delta) - B'_2\sin(2\delta)x + C'x^2\right]}{A'' - \left[B''_1\cos(2\delta) - B''_2\sin(2\delta)x + C''x^2\right]} + \frac{A'''x^2}{\left\{A'' - \left[B''_1\cos(2\delta) - B''_2\sin(2\delta)x + C''x^2\right]\right\}} \times \frac{1}{\left\{D'' - \left[E''_1\cos(2\delta) - E''_2\sin(2\delta)x + F''x^2\right]\right\}}, \tag{5}$$

where:

$$A' = \left[(n-1)^2 + \kappa^2\right]\left[(n+n_s)^2 + \kappa^2\right], \tag{6a}$$

$$B'_1 = 2\left[\left(n^2 + \kappa^2 - 1\right)\left(n^2 + \kappa^2 - n_s^2\right) + 4\kappa^2 n_s\right], \tag{6b}$$

$$B'_2 = 4\kappa\left[n_s\left(n^2 + \kappa^2 - 1\right) - \left(n^2 + \kappa^2 - n_s^2\right)\right], \tag{6c}$$

$$C' = \left[(n+1)^2 + \kappa^2\right]\left[(n-n_s)^2 + \kappa^2\right], \tag{6d}$$

$$A'' = \left[(n+1)^2 + \kappa^2\right]\left[(n+n_s)^2 + \kappa^2\right], \tag{6e}$$

$$B''_1 = 2\left[\left(n^2 + \kappa^2 - 1\right)\left(n^2 + \kappa^2 - n_s^2\right) - 4\kappa^2 n_s\right], \tag{6f}$$

$$B''_2 = 4\kappa\left[n_s\left(n^2 + \kappa^2 - 1\right) + \left(n^2 + \kappa^2 - n_s^2\right)\right], \tag{6g}$$

$$C'' = \left[(n-1)^2 + \kappa^2\right]\left[(n-n_s)^2 + \kappa^2\right], \tag{6h}$$

$$A''' = 64n_s(n_s - 1)^2\left(n^2 + \kappa^2\right)^2, \tag{6i}$$

$$D'' = \left[(n+1)^2 + \kappa^2\right]\left[(n+1)\left(n + n_s^2\right) + \kappa^2\right], \tag{6j}$$

$$E''_1 = 2\left[\left(n^2 + \kappa^2 - 1\right)\left(n^2 + \kappa^2 - n_s^2\right) - 2\kappa^2\left(n_s^2 + 1\right)\right], \tag{6k}$$

$$E''_{12} = 2\kappa\left[\left(n^2 + \kappa^2 - n_s^2\right) + \left(n_s^2 + 1\right)\left(n^2 + \kappa^2 - 1\right)\right], \tag{6l}$$

$$F'' = \left[(n-1)^2 + \kappa^2\right]\left[(n-1)\left(n - n_s^2\right) + \kappa^2\right]. \tag{6m}$$

and:

$$T = \frac{Ax}{B - [C\cos(2\delta) - D\sin(2\delta)]x + Ex^2}, \tag{7}$$

where:

$$A = 16n_s\left(n^2 + \kappa^2\right), \tag{8a}$$

$$B = \left[(n+1)^2 + \kappa^2\right]\left[(n+1)\left(n + n_s^2\right) + \kappa^2\right], \tag{8b}$$

$$C = 2\left[\left(n^2 - 1 + \kappa^2\right)\left(n^2 - n_s^2 + \kappa^2\right) - 2\kappa^2\left(n_s^2 + 1\right)\right], \tag{8c}$$

$$D = 2\kappa\left[2\left(n^2 - n_s^2 + \kappa^2\right) + \left(n_s^2 + 1\right)\left(n^2 - 1 + \kappa^2\right)\right], \tag{8d}$$

$$E = \left[(n-1)^2 + \kappa^2\right]\left[(n-1)\left(n - n_s^2\right) + \kappa^2\right]. \tag{8e}$$

$$\delta = 2\pi nd/\lambda \tag{8f}$$

$$x = \exp(-\alpha d) \tag{8g}$$

$$\alpha = 4\pi\kappa/\lambda \tag{8h}$$

In practice, it is much simpler to use experimental measurement of transmission spectra (or transmittance) to obtain parameters describing the optical constants of the tested material [39–41].

Measurements of the transmission spectra of the tested thin layers were performed in a wide range from 200 to 3000 nm using double beams PerkinElmer's LAMBDA950 UV/Vis/NIR Spectrophotometer with a resolution of 1 nm [42]. To measure the temperature dependence of the transmission spectra, a top-class Analytik Jena UV/Vis/NIR spectrophotometer cooperating with a Janis SuperTran-VP cryostat (cooling agent - liquid nitrogen) and a Lake Shore Cryotronics temperature controller was used. Temperature measurements were performed with a resolution of 1 nm in the range from 200 to 1100 nm.

Fig. 6 shows the experimental spectrum for a homogeneous $CH_3NH_3PbI_3$ hybrid perovskite film deposited on a transparent glass

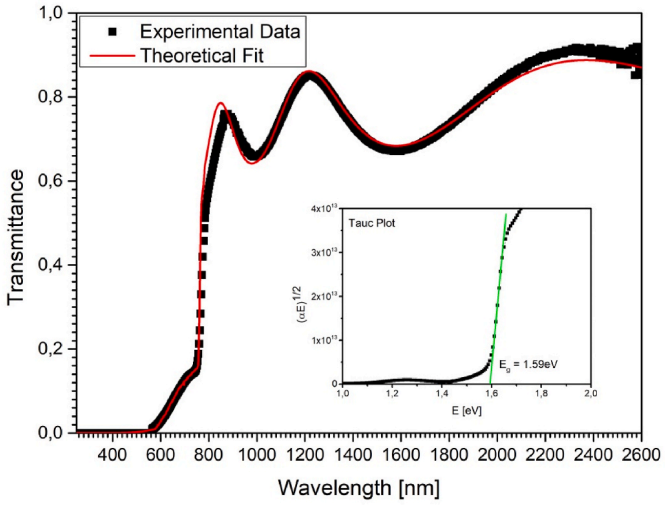


Fig. 6. Chart the experimental transmittance spectrum and theoretical fit (based on equations (7) and (8)) of the thin hybrid perovskite film ($CH_3NH_3PbI_3$) fabricated by PVco-D on a glass substrate (BK7). The inner plot shows the Tauc plot.

substrate. The obtained experimental spectrum is divided into two parts: strong (range 200–740 nm) and weak (range 740–2600 nm) absorption and agrees perfectly with the results of transmission obtained for methylammonium lead iodide crystals [43]. The graph also clearly shows oscillations resulting from interference after light passes through the tested layer + substrate system. These oscillations, in accordance with equations (7) and (8), were used to determine material constants, such as refractive index n, absorption α and extinction coefficients κ, complex dielectric constant $\varepsilon = \varepsilon_r + \varepsilon_i$ and optical energy gap E_g. The dependences of the refractive index n, absorption coefficient α, extinction coefficient κ and the complex dielectric constant as a function of the wavelength in the UV-VIS-NIR range are shown in Fig. 7.

The curve showing the change in the refractive index (black color) as a function of wavelength has a typical dispersion curve character. The estimated value of the refractive index at wavelengths approaching infinity outside the strong absorption region converges to a value of approximately 2.15. This result is equal to the value of the refractive index of the $CH_3NH_3PbI_3$ crystals [42]. The analysis of the curves illustrating the behavior of the absorption and extinction coefficients (pink and green colors, respectively) indicates a clear division into the ranges of strong absorption and its almost complete absence. The absorption limit occurs at a wavelength of 740 nm. Above this value, the tested layers of organic-inorganic halide perovskite were transparent. This leads to the conclusion that if solar cells use only the hybrid perovskite absorption layer, they will not absorb the entire infrared

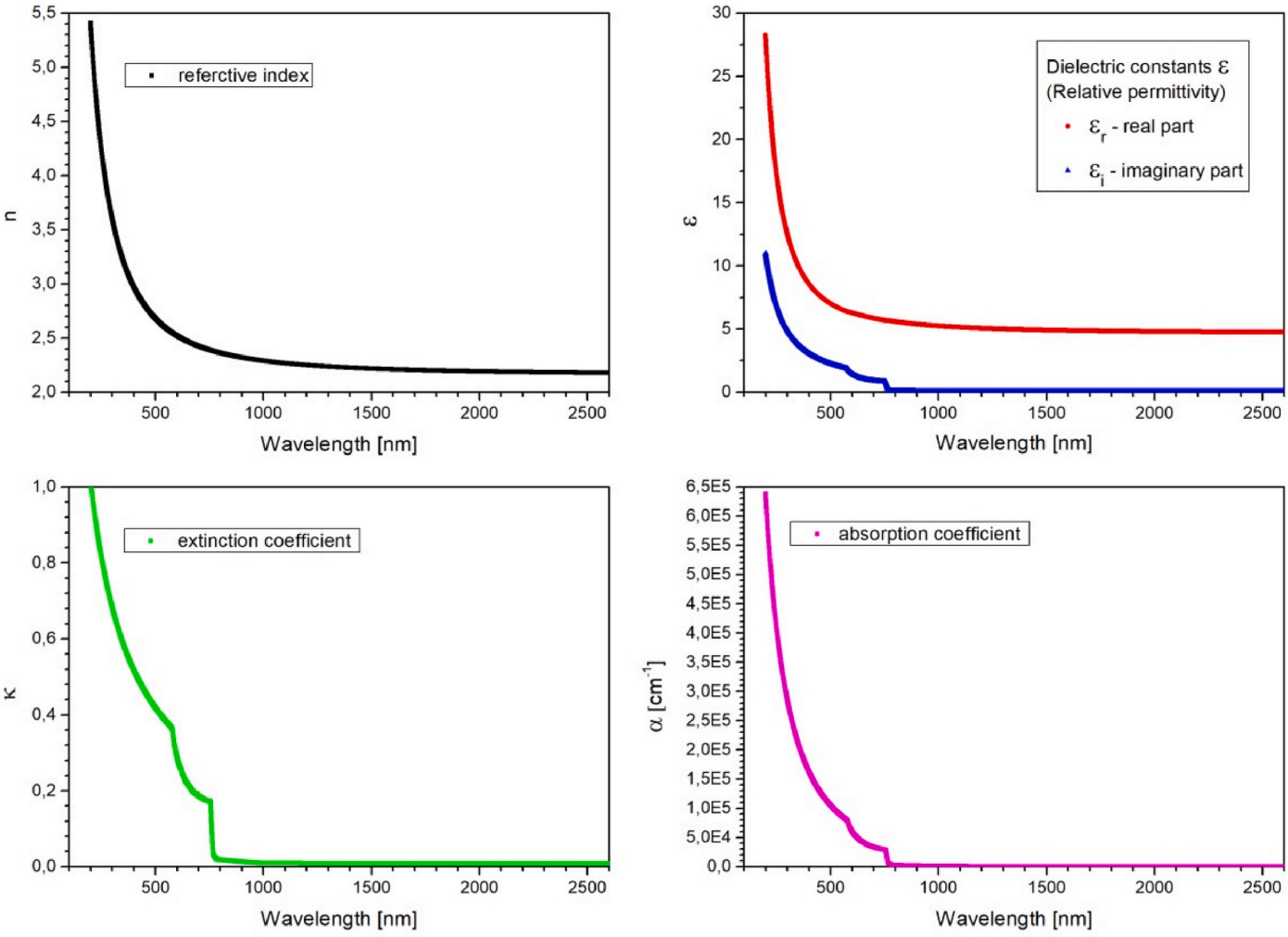


Fig. 7. Graphs of basic physical parameters characterizing perovskite film ($CH_3NH_3PbI_3$) calculated on the basis of theoretical fit (Eqs. (7) and (8)) and experimental data.

spectrum but only a small part of it.

The relationships describing the behavior of the refractive index and extinction coefficient were used to determine the complex dielectric constant $\varepsilon = \varepsilon_r + i\varepsilon_i$, where $\varepsilon_r = |\tilde{n}|^2 = n^2 - \kappa^2$ and $\varepsilon_i = 2n\kappa$. Since this quantity is closely related to the extinction and refraction coefficients, both its components and the modulus will reflect their nature. It causes the complex dielectric constant to be equal to its real part outside the strong absorption region. In the absorption area, both components are essential, but the contribution of the imaginary component is significantly smaller. The estimated value of the dielectric constant at wavelengths approaching the strong absorption region converges to a value of approximately 4.8. This result agrees with the value of the dielectric constant of the $CH_3NH_3PbI_3$ crystals equal to 5 [43].

Fig. 8 shows the changes occurring in the transmission spectrum of the methylammonium lead iodide layers under the influence of temperature in visible and near-infrared range, considering the edges of the adsorption band. Within the selected range, the temperature changed from the temperature of liquid nitrogen to room temperature, and experimental measurements were performed every 10 K after the appropriate temperature had stabilized.

The analysis of the measurement data of the transmission spectra led to several extremely interesting conclusions. The basic information presented by experimental spectra is that changes in temperature result in a shift of the edge of the absorption band and a related change in the value of the optical energy gap. The shifting of the edge of the absorption band, depending on the temperature, may change gently or abruptly. For the layers obtained using the PVco-D process examined in this work, mild changes occur in two ranges: from room temperature to approximately 130 K and temperatures below 100 K. However, the changes become abrupt in the range of 100–130 K. The observed direction of changes is surprising - as the temperature decreases, the optical energy gap decreases (in both ranges 77–100 K and 130–300 K). Such a relationship is not typical for materials, e.g., in organic and inorganic semiconductor materials, the behavior is opposite; a drop in temperature causes an increase in the optical value of energy gaps. A graphical method of determining E_g known as Tauc plots was used to conduct a thorough analysis.

In this method, the absorption coefficient is analyzed depending on the energy of the incident radiation near the absorption edge. This allows us to determine the optical energy gap and the type of optical transition for both crystalline and non-crystalline materials. Based on dependencies (Eq. (9)), the optical energy gap was estimated:

$$\alpha h\frac{c}{\lambda} = a'\left(\frac{hc}{\lambda} - E_g\right)^f, \tag{9}$$

where: h is Planck's constant, c - the speed of light, E_g is the energy gap value, $f = 1/2$ or $f = 3/2$ for a direct allowed or direct forbidden optical transition and $f = 2$ or $f = 3$ for an indirect allowed or indirect forbidden optical transition, appropriately. The constant a' is a parameter that depends on the optical transition probability and characterizes the material. The best fit of the experimental data was obtained for $f = 1/2$, which corresponds to the absorption edge of the direct allowed optical transition. Fig. 6 (internal plot) shows the analysis of the $\alpha h\frac{c}{\lambda}$ relationship as a function of $a'\left(\frac{hc}{\lambda} - E_g\right)^{1/2}$ in the absorption band edge

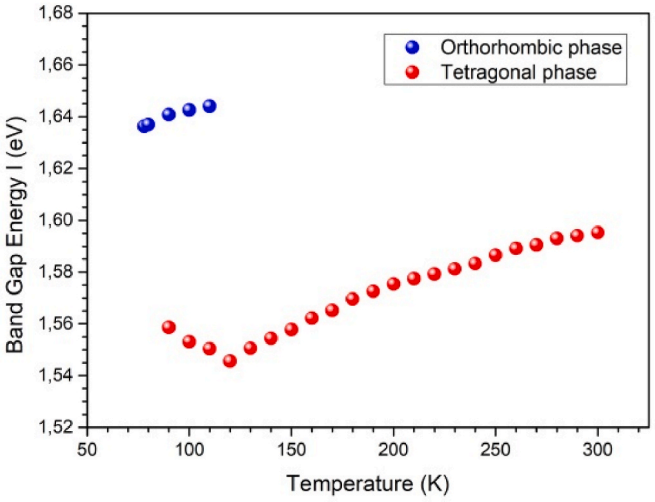


Fig. 9. Temperature dependence of the optical energy gap E_g for $MAPbI_3$ film.

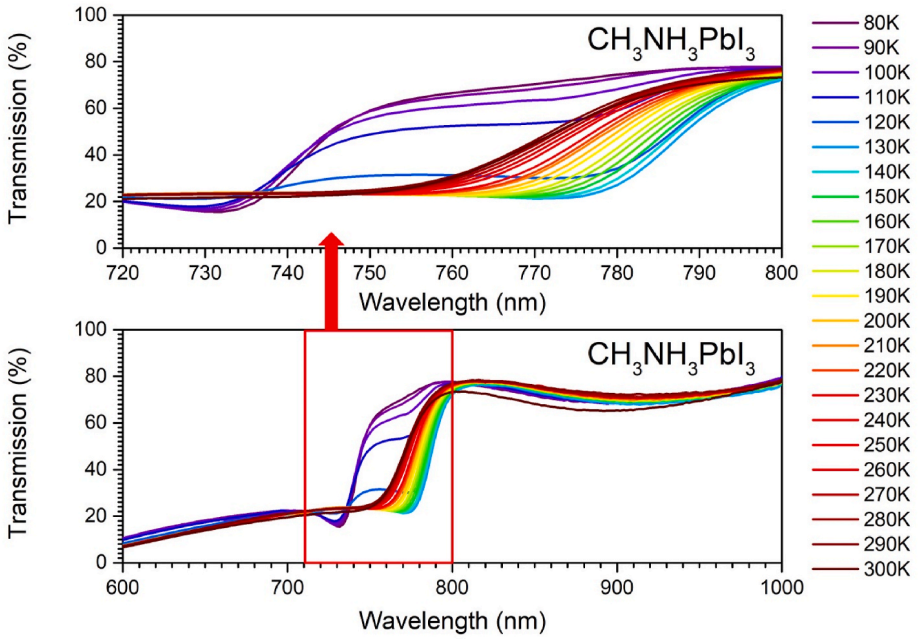


Fig. 8. Temperature dependence of the transmission spectrum for *MAPbI3 film* in the VIS and NIR region (the upper graph is an enlargement of a fragment of the spectrum).

region. Individual transmission spectra obtained for different temperatures were analyzed using Tauc Plots. The obtained values of the optical energy gap E_g are presented in Fig. 9.

The estimated optical energy gap values suggest that for $MAPbI_3$ layers produced by the PVco-D deposition process, the phase transition from the orthorhombic phase to the tetragonal phase occurs at a lower temperature than in the case of bulk crystals and layers deposited from solution in the spin coating process. In the case under consideration, the temperature range should be indicated as 100–130 K, not a single value. A detailed analysis of the transmission spectra indicates that both phases can coexist in this temperature range. It leads to the conclusion that the technique used to deposit thin layers of hybrid perovskites influences their properties. The films obtained in the PVco-D process have a higher density than those obtained from the solution. They are also more uniform over a relatively large surface. Continuously lowering the temperature of the material in the tetragonal phase leads to stresses and stretches inside the structure. The compact crystallographic structure is more resistant to emerging stresses and does not allow for a simultaneous phase change related to the movement of atoms in the unit cell. Similar behavior can be expected when transitioning from the tetragonal to cubic phase.

4.3. Photoluminescence and its temperature dependence

The temperature dependence of the photoluminescence spectra of the tested thin films was measured in a range from 190 to 1100 nm using an Exemplar® Plus LS B&WTek Spectrometer captured spectra with a resolution of 0.6 nm working with a Janis cryostat (cooling agent - liquid helium, temperature range: 10–320 K) and a temperature controller Lake Shore Cryotronics and also in a range from 300 to 1000 nm using a FluoroMax-4P HORIBA Spectrofluorometers working with a Janis SuperTran-VP cryostat (cooling agent - liquid nitrogen, temperature range: 77–300 K) and a temperature controller Lake Shore Cryotronics [44].

Fig. 10a–b shows experimental 3D PL spectra for a homogeneous $CH_3NH_3PbI_3$ hybrid perovskite layer deposited on a transparent glass substrate, measured at liquid nitrogen and room temperature using FluoroMax-4P equipment.

Analysis of the presented 3D PL spectra shows that the intensity of the generated photoluminescence changes significantly as a function of temperature. At 77 K, it is six times stronger than at room temperature – moreover, the position of both the emission and excitation maximum changes. As the temperature decreases, the emission spectrum shifts slightly towards shorter wavelengths, and the shift value is approximately 30 nm. However, the shift of the excitation maximum is much more significant and amounts to about 170 nm; similarly to the emission, the excitation maximum shifts towards shorter wavelengths.

Due to the significant difference in emission intensities as a function of photoluminescence temperature measurement, detailed studies were carried out. The emission characteristics were measured at an excitation wavelength of 450 nm, an intermediate value between the excitation maximums for temperatures of 77 K and 300 K, and due to the lower photoluminescence intensity being closer to the max at room temperature.

Fig. 11a–b shows the experimental results of photoluminescence changes obtained from measurements in the temperature range from 10 to 320 K (Exemplar® Plus LS Spectrometer). The measurement results allowed us to observe a significant intensity of photoluminescence in the temperature range of 10–110 K (Fig. 11a), and the highest maximum intensity was obtained at the temperature of 90 K. In the range of the observed strong PL intensity, the shift in the position of the absolute PL maximum is 40 K, and this value corresponds to the range of changes in the position of the absorption boundary observed in the transmission spectra. However, it is shifted by about 20 K towards lower temperatures. The highest photoluminescence intensity was obtained in the temperature range close to the phase transition temperature between the tetragonal and orthorhombic phases. It allows us to conclude that photoluminescence in thin layers of methylammonium lead iodide may be related to stresses and/or stretches within the crystal structure, which explains the difference in our observations compared to layers obtained from DMF solutions containing hybrid perovskite precursors with a much shorter structure order [45].

Normalizing the intensity of the PL spectra allowed us to observe the spectra' shape, the maximum's location, and its movement as a function of temperature. Due to the shape of the spectrum, the experimental results can be divided into two ranges: 10–140 K, where the individual spectra have a complex form and have been approximated to two Gaussian functions, and 150–320 K, where the spectra have a simplified shape and despite the approximation to two Gaussian functions, only one dominates (the second one practically disappears). In the first temperature interval of 10–140 K, the first peak (Peak 1 – Maximum at 746 nm) monotonically shifts towards shorter wavelengths with increasing temperature. However, the second peak (Peak 2 – Maximum at 775 nm) initially (10–70 K) also monotonically goes towards shorter

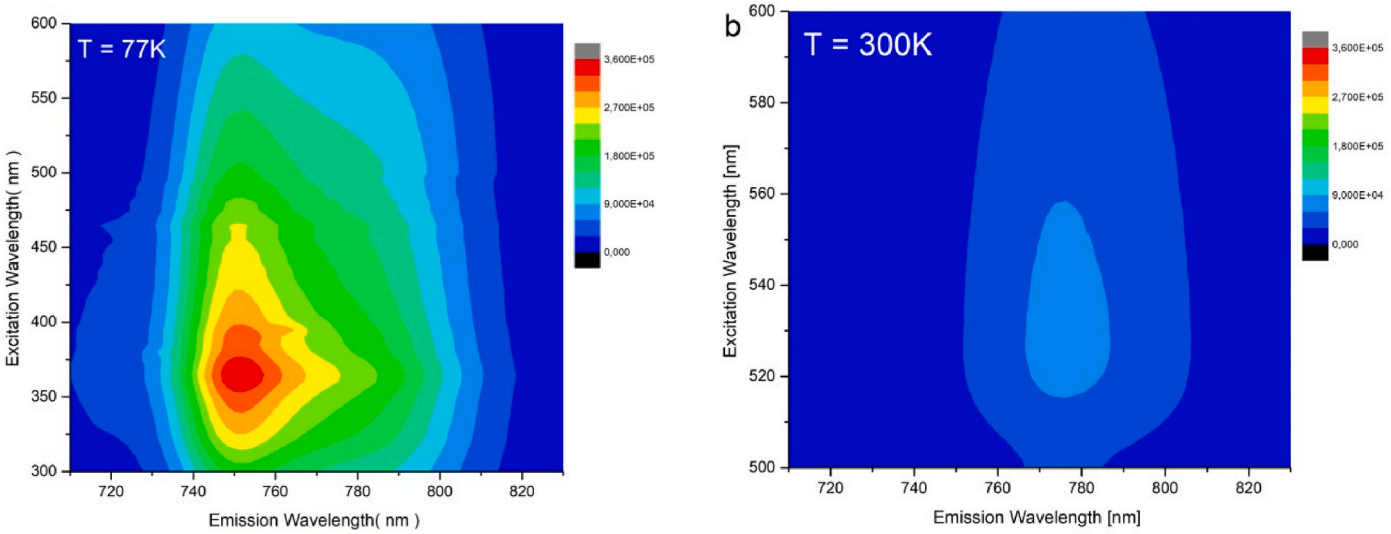


Fig. 10. Experimental 3D photoluminescence spectra of the $MAPbI_3$ thin film (colors represent emission intensity): (a) at the temperature of liquid nitrogen – 77 K and (b) at room temperature – 300 K.

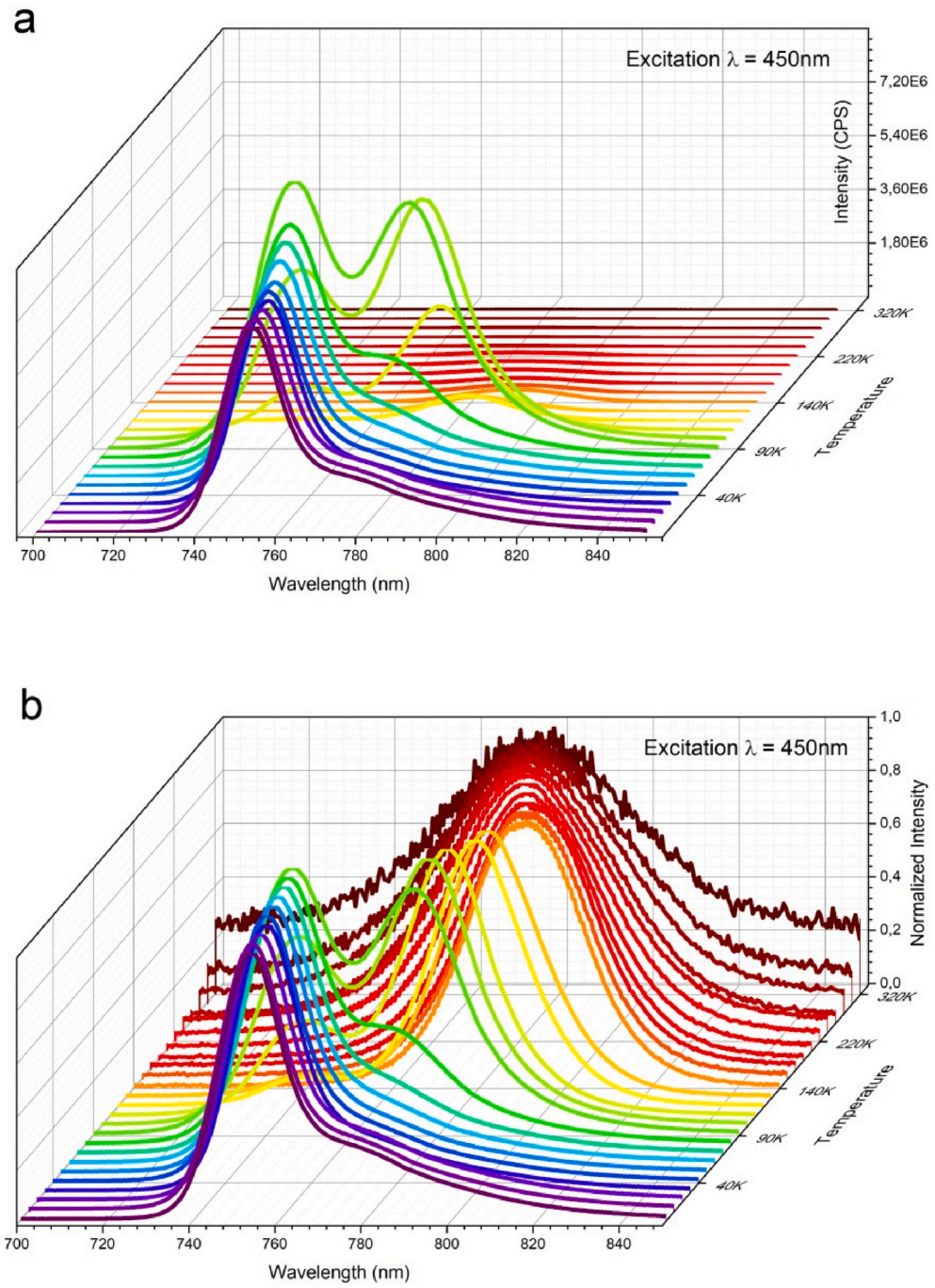


Fig. 11. Experimental PL spectra of the $MAPbI_3$ thin film as a function of the temperature: taking into account PL intensity values (a) and normalized to the maximum PL intensity value (b).

wavelengths and then changes direction and monotonically shifts towards longer wavelengths. The maximum wavelength corresponding to the Gaussian maximum for the second peak is observed at 150 K. In the second temperature interval of 150–320 K, the first peak (Peak 1) practically disappears. In contrast, the second peak (Peak 2) monotonically shifts towards shorter wavelengths until the end of the temperature measurement range. Fig. 12a–b shows the results of fitting two Gaussian functions in the temperature range 10–320 K. Based on the results obtained, in the temperature range where the phase change from orthorhombic to tetragonal occurs, the displacement of the second peak is complicated. The first peak in the luminescence spectrum is most likely related to the orthorhombic crystallographic phase, while the second one is associated with the tetragonal phase. However, it should be noted that the second peak occurs throughout the entire measurement range.

4.4. *Resistance - temperature and lighting dependencies*

The temperature dependence of the resistance of MAPbI3 thin films was measured from 10 to 300 K. The experimental setup included the KEITHLEY 4200-scs measuring system, equipped with three SMU (Source Measurement Unit) units allowed us to analyze the electrical parameters of the tested structures. The SMU can work as a voltage or current source (depending on the selected function) and is connected in